3

QCD in electron-positron annihilation

Many of the basic ideas and properties of perturbative QCD can be illustrated by considering the production of hadrons in electron-positron annihilation. In this chapter we will discuss a variety of ways in which the theory can be tested. We begin by discussing the *total cross section* for $e^+e^- \to$ hadrons: we show how the order α_S corrections are calculated, and how renormalization scheme dependence enters at order α_S^2. Because of its inclusive nature, this is one of the few quantities for which the first three terms in the QCD perturbation series are known, and for which non-perturbative corrections are expected to be small. As a result it provides potentially one of the most precise measurements of the strong coupling.

Perturbative QCD also predicts a rich 'jet' structure for the final-state hadrons in electron-positron annihilation. We discuss the various ways in which jet cross sections can be defined, how such cross sections are calculated in perturbation theory, and how the predictions compare with experiment. Jet cross sections can also be used to measure α_S, and to test the basic interactions in the theory, in particular the triple-gluon vertex.

3.1 The total hadronic cross section

The production of a muon pair in electron-positron annihilation, $e^+e^- \to \mu^+\mu^-$, is one of the fundamental processes of QED. The same annihilation process can also produce hadrons in the final state. As we have seen in the previous chapter, the formation of these hadrons is not governed by perturbation theory. Why then would one expect a perturbative approach to give an accurate description of the hadronic cross section? The answer can be understood by visualizing the event in space-time. The electron

Downloaded from https://www.cambridge.org/core. UNIVERSIDAD AUTONOMA METROPOLITANA, on 15 Nov 2026 at 06:22:37, subject to the Cambridge Core terms of use, available at https://www.cambridge.org/core/terms. https://doi.org/10.1017/CBO9780511628788.004

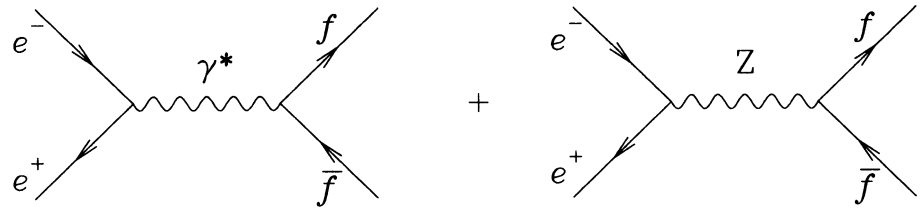


Fig. 3.1. Feynman diagrams for the process $e^+e^- \to f\bar{f}$.

and positron form a photon (or Z), of virtuality Q equal to the collision energy $\sqrt{s}$, which fluctuates into a quark and an antiquark. By the uncertainty principle, this fluctuation occurs on a distance scale of order $1/Q$, and if Q is large the production rate for this short-distance process should be predicted by perturbation theory. Subsequently, the quarks and gluons form themselves into hadrons. This process is called *hadronization*. Hadronization occurs at a much later time scale characterized by $1/\Lambda$, where Λ is the scale in α_S, *i.e.* the scale at which the coupling becomes strong. The interactions which change quarks and gluons into hadrons certainly modify the outgoing state, but they occur too late to modify the original probability for the event to happen, which can therefore be calculated in perturbation theory.

At lowest order, the total hadronic cross section is obtained by simply summing over all kinematically accessible flavours and colours of quark-antiquark pairs, $e^+e^- \to \sum q\bar{q}$. Real and virtual gluon corrections to this basic process will generate higher-order contributions to the perturbation series. Since it is convenient to compare the hadronic cross section to that for $\mu^+\mu^-$ production, and to include the possibility of both photon and Z exchange, we begin by considering the general high-energy $2 \to 2$ process $e^+e^- \to f\bar{f}$, with f a light charged fermion, $f \neq e$. At lowest order, this is mediated by either a virtual photon or a Z in the s-channel, Fig. 3.1. With θ the centre-of-mass scattering angle of the final-state fermion, the differential cross section is

$$\begin{aligned}\frac{d\sigma}{d\cos\theta} &= \frac{\pi\alpha^2}{2s}\Big[(1+\cos^2\theta)\Big\{Q_f^2 - 2Q_fV_eV_f\chi_1(s) \\ &\quad + (A_e^2+V_e^2)(A_f^2+V_f^2)\chi_2(s)\Big\} \\ &\quad + \cos\theta\Big\{-4Q_fA_eA_f\chi_1(s) + 8A_eV_eA_fV_f\chi_2(s)\Big\}\Big] \,, \quad (3.1)\end{aligned}$$

where

$$\chi_1(s) = \kappa\,\frac{s(s-M_Z^2)}{(s-M_Z^2)^2+\Gamma_Z^2M_Z^2}$$

Downloaded from https://www.cambridge.org/core. UNIVERSIDAD AUTONOMA METROPOLITANA, on 15 Nov 2026 at 06:22:37, subject to the Cambridge Core terms of use, available at https://www.cambridge.org/core/terms. https://doi.org/10.1017/CBO9780511628788.004

$$\chi_2(s) = \kappa^2 \frac{s^2}{(s-M_Z^2)^2+\Gamma_Z^2 M_Z^2}$$
$$\kappa = \frac{\sqrt{2}G_F M_Z^2}{16\pi\alpha} . \tag{3.2}$$

Here G_F is the Fermi constant, α is the electromagnetic coupling, and M_Z and Γ_Z are the mass and total decay width of the Z boson respectively. The vector and axial couplings of the fermions to the Z are (see Chapter 8)

$$V_f = T_f^3 - 2Q_f \sin^2\theta_W , \quad A_f = T_f^3 , \tag{3.3}$$

with $T_f^3 = +\frac{1}{2}$ for $f = \nu,\ u,\ \ldots$ and $T_f^3 = -\frac{1}{2}$ for $f = e,\ d,\ \ldots$. The χ_2 term comes from the square of the Z-exchange amplitude and the χ_1 term from the photon-Z interference. At centre-of-mass scattering energies ($\sqrt{s}$) far below the Z peak, the ratio s/M_Z^2 is small and so $1 \gg \chi_1 \gg \chi_2$. This means that the weak effects — manifest in the terms involving the vector and axial couplings — are small and can be neglected. Eq. (3.1) then reduces to

$$\frac{d\sigma}{d\cos\theta} = \frac{\pi\alpha^2 Q_f^2}{2s}(1+\cos^2\theta) . \tag{3.4}$$

Integrating over θ gives the total cross section,

$$\sigma_0 = \frac{4\pi\alpha^2}{3s} Q_f^2 . \tag{3.5}$$

On the Z pole, $\sqrt{s} = M_Z$, the χ_2 term in (3.1) dominates and the corresponding (peak) cross section is

$$\sigma_0 = \frac{4\pi\alpha^2\kappa^2}{3\Gamma_Z^2}(A_e^2+V_e^2)(A_f^2+V_f^2) . \tag{3.6}$$

We next introduce the ratio R of the total e^+e^- hadronic cross section to the muon pair production cross section. As we have argued, the hadronic cross section is obtained at leading order simply by counting the possible $q\bar{q}$ final states. Thus, at energies far below the Z pole, we have (*cf.* Eq. (1.7))

$$R = \frac{\sigma(e^+e^- \to \text{hadrons})}{\sigma(e^+e^- \to \mu^+\mu^-)} = \frac{\sum_q \sigma(e^+e^- \to q\bar{q})}{\sigma(e^+e^- \to \mu^+\mu^-)} = 3\sum_q Q_q^2 , \tag{3.7}$$

where the factor 3 comes from the sum over quark colours. On the Z pole, the analogous quantity is the ratio of the partial decay widths of the Z to hadrons and to muon pairs:

$$R_Z = \frac{\Gamma(Z \to \text{hadrons})}{\Gamma(Z \to \mu^+\mu^-)} = \frac{\sum_q \Gamma(Z \to q\bar{q})}{\Gamma(Z \to \mu^+\mu^-)} = \frac{3\sum_q (A_q^2+V_q^2)}{A_\mu^2+V_\mu^2} . \tag{3.8}$$

Downloaded from https://www.cambridge.org/core. UNIVERSIDAD AUTONOMA METROPOLITANA, on 15 Nov 2026 at 06:22:37, subject to the Cambridge Core terms of use, available at https://www.cambridge.org/core/terms. https://doi.org/10.1017/CBO9780511628788.004

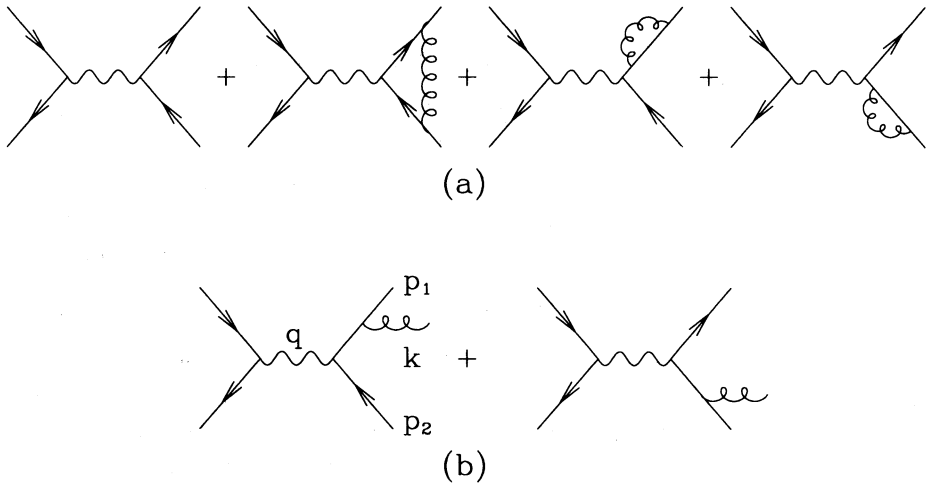


Fig. 3.2. Feynman diagrams for the $O(\alpha_S)$ corrections to the total hadronic cross section in e^+e^- annihilation.

These results are valid for massless quarks; the effect of a non-zero quark mass will be discussed in Section 3.2.

With $q = u, \ldots, b$, Eq. (3.7) gives $R = 11/3 = 3.67$ and (with $\sin^2\theta_W = 0.23$) $R_Z = 20.09$. For the latter, the measured value at LEP is 20.79 ± 0.04 [1], some 3.5% higher than the lowest-order prediction. In fact the difference is largely due to higher-order QCD corrections, and the comparison between theory and experiment provides a determination of the strong coupling constant, as we shall see in Chapter 12.

The $O(\alpha_S)$ corrections to the total hadronic cross section are calculated from the real and virtual gluon diagrams shown in Fig. 3.2. For simplicity, we shall consider only the photon-exchange contribution in detail. For the real gluon diagrams, Fig. 3.2(b), it is convenient to write the three-body phase space integration as

$$d\Phi_3 = \frac{1}{(2\pi)^5}\,\frac{s}{32}\,d\alpha\,d\cos\beta\,d\gamma\,dx_1\,dx_2\,, \tag{3.9}$$

where α, β, γ are Euler angles, and $x_1 = 2E_q/\sqrt{s}$ and $x_2 = 2E_{\bar{q}}/\sqrt{s}$ are the energy fractions of the final-state quark and antiquark. The matrix element squared for $e^+(q_1) + e^-(q_2) \to q(p_1) + \bar{q}(p_2) + g(k)$ is obtained using the Feynman rules given in Chapter 1:

$$\frac{1}{4}\sum|\mathcal{M}|^2 = 24C_F e^4 Q_q^2 g_s^2 \frac{(p_1\cdot q_1)^2 + (p_1\cdot q_2)^2 + (p_2\cdot q_1)^2 + (p_2\cdot q_2)^2}{q_1\cdot q_2\; p_1\cdot k\; p_2\cdot k}\,, \tag{3.10}$$

where the sum is over spins and colours. If we integrate out the Euler angles then the matrix element depends only on x_1 and x_2. The contribution

Downloaded from https://www.cambridge.org/core. UNIVERSIDAD AUTONOMA METROPOLITANA, on 15 Nov 2026 at 06:22:37, subject to the Cambridge Core terms of use, available at https://www.cambridge.org/core/terms. https://doi.org/10.1017/CBO9780511628788.004

to the total cross section is then

$$\sigma^{q\bar{q}g} = \sigma_0 \, 3 \sum_q Q_q^2 \int dx_1 dx_2 \, C_F \frac{\alpha_S}{2\pi} \frac{x_1^2 + x_2^2}{(1-x_1)(1-x_2)} \tag{3.11}$$

where $\sigma_0 = 4\pi\alpha^2/(3s)$ and the integration region is: $0 \leq x_1, x_2 \leq 1$, $x_1 + x_2 \geq 1$. Unfortunately, the integrals in Eq. (3.11) are divergent along the boundaries at $x_i = 1$. Since $1 - x_1 = x_2 E_g (1 - \cos\theta_{2g})/\sqrt{s}$ and $1 - x_2 = x_1 E_g (1 - \cos\theta_{1g})/\sqrt{s}$, where E_g is the gluon energy and θ_{ig} $(i = 1, 2)$ the angles between the gluon and the quarks, we see that the singularities come from regions of phase space where the gluon is *collinear* with the quark or antiquark, $\theta_{ig} \to 0$, or where the gluon is *soft*, $E_g/\sqrt{s} \to 0$. These singularities are not of course physical; they simply indicate a breakdown of the perturbative approach. Quarks and gluons are never on-mass-shell particles, as this calculation assumes. When we encounter gluon energies and quark-gluon invariant masses which are of the same order as hadronic mass scales (~ 1 GeV or less) then we cannot ignore the effects of confinement. We will discuss in later chapters various ways to model these effects. In the meantime, we can regard the singular behaviour on the boundaries of the phase space diagram as signifying physics beyond perturbation theory.

The key point is that we have not yet demonstrated that these 'dangerous' regions actually make an important contribution to the total cross section. The way to proceed is to introduce a temporary 'regularization procedure' for making the integrals finite, both for the real- and virtual-gluon diagrams, and then to see whether we can remove the regulator at the end of the calculation and obtain a finite result. Several methods are suitable. We can give the gluon a small mass, or take the final-state quark and antiquark off mass-shell by a small amount (which one might argue had some physical relevance). With either of these procedures, the singularities in the contributions from individual diagrams are avoided, being manifest instead as logarithms of the regulating mass scale.

A mathematically more elegant regularization procedure is to use dimensional regularization, with the number of space-time dimensions now $n > 4$. Recall that this was encountered in the previous chapter as a method for performing ultraviolet regularization in the context of renormalization. Here the method is being extended to *real* gluon emission in addition to loop diagrams. Going to $n \neq 4$ dimensions affects both the phase space and the traces of the Dirac matrices in the $q\bar{q}g$ cross-section calculation. As a result, Eq. (3.11) becomes

$$\sigma^{q\bar{q}g}(\epsilon) = \sigma_0 \, 3 \sum_q Q_q^2 \, H(\epsilon) \int dx_1 dx_2 \, \frac{2\alpha_S}{3\pi} \frac{x_1^2 + x_2^2 - \epsilon(2 - x_1 - x_2)}{(1-x_1)^{1+\epsilon}(1-x_2)^{1+\epsilon}} \tag{3.12}$$

Downloaded from https://www.cambridge.org/core. UNIVERSIDAD AUTONOMA METROPOLITANA, on 15 Nov 2026 at 06:22:37, subject to the Cambridge Core terms of use, available at https://www.cambridge.org/core/terms. https://doi.org/10.1017/CBO9780511628788.004

with $\epsilon = \frac{1}{2}(4-n)$, and

$$H(\epsilon) = \frac{3(1-\epsilon)^2}{(3-2\epsilon)\Gamma(2-2\epsilon)} = 1 + O(\epsilon) \,, \tag{3.13}$$

where Γ is the Euler gamma function given in Eq. (2.57). With the three-body phase space integrals recast in n dimensions, the soft and collinear singularities are regulated, appearing instead as *poles* at $n = 4$. Performing the integrations in Eq. (3.12) gives

$$\sigma^{q\bar{q}g}(\epsilon) \;=\; \sigma_0 \, 3 \sum_q Q_q^2 \, \frac{\alpha_S}{2\pi} \, H(\epsilon) \, \left[\frac{2}{\epsilon^2} + \frac{3}{\epsilon} + \frac{19}{2} + O(\epsilon) \right] . \tag{3.14}$$

The virtual gluon contribution can be calculated in a similar fashion, with dimensional regularization again used to control the infra-red divergences in the loops. The result is

$$\sigma^{q\bar{q}(g)}(\epsilon) \;=\; \sigma_0 \, 3 \sum_q Q_q^2 \, \frac{C_F \alpha_S}{2\pi} \, H(\epsilon) \, \left[-\frac{2}{\epsilon^2} - \frac{3}{\epsilon} - 8 + O(\epsilon) \right] . \tag{3.15}$$

When the two contributions Eqs. (3.14) and (3.15) are added together, the poles exactly cancel and the result is *finite* in the limit $\epsilon \to 0$:

$$R \;=\; 3 \sum_q Q_q^2 \, \left\{ 1 + \frac{\alpha_S}{\pi} + O(\alpha_S^2) \right\} . \tag{3.16}$$

At this order and for massless quarks, the QCD correction is independent of the nature of the exchanged weak boson, *i.e.* the $1 + \alpha_S/\pi$ result is valid also for R_Z. Notice also that the next-to-leading-order correction is positive, and with a value for α_S of about 0.11, can accommodate the experimental measurement of R_Z given above. In contrast, the corresponding correction would be negative in a theory with a scalar gluon.

The cancellation of the soft and collinear singularities between the real and virtual gluon diagrams is not accidental. There are theorems — the Bloch, Nordsieck [2] and Kinoshita, Lee, Nauenberg [3] theorems — which state that suitably defined inclusive quantities will indeed be free of singularities in the massless limit. The total hadronic cross section is an example of such a quantity, whereas the cross section for the exclusive $q\bar{q}$ final state, *i.e.* $\sigma(e^+e^- \to q\bar{q})$ with no gluon emission, is not.

In the above result, the coupling α_S is understood to be evaluated at a renormalization scale μ. Since the ultraviolet divergences in the loop diagrams in Fig. 3.2 cancel, the coefficient of the coupling is independent of μ at this order. At $O(\alpha_S^2)$ and higher, we encounter the ultraviolet divergences associated with the renormalization of the strong coupling. The coefficients are therefore renormalization scheme dependent, and we

Downloaded from https://www.cambridge.org/core. UNIVERSIDAD AUTONOMA METROPOLITANA, on 15 Nov 2026 at 06:22:37, subject to the Cambridge Core terms of use, available at https://www.cambridge.org/core/terms. https://doi.org/10.1017/CBO9780511628788.004

can write (see Chapter 2)

$$\begin{aligned} R &= K_{QCD}\, 3 \sum_q Q_q^2, \\ K_{QCD} &= 1 + \frac{\alpha_S(\mu^2)}{\pi} + \sum_{n\geq 2} C_n \left(\frac{s}{\mu^2}\right) \left(\frac{\alpha_S(\mu^2)}{\pi}\right)^n . \end{aligned} \tag{3.17}$$

The $O(\alpha_S^2)$ and $O(\alpha_S^3)$ corrections have been calculated. In the $\overline{\rm MS}$ scheme with the renormalization scale choice $\mu = \sqrt{s}$, the values are

$$\begin{aligned} C_2(1) &= \left(\frac{2}{3}\zeta(3) - \frac{11}{12}\right) n_f + \left(\frac{365}{24} - 11\zeta(3)\right) \\ &\simeq 1.986 - 0.115 n_f \\ C_3(1) &= \left(\frac{87029}{288} - \frac{1103}{4}\zeta(3) + \frac{275}{6}\zeta(5)\right) \\ &\quad - \left(\frac{7847}{216} - \frac{262}{9}\zeta(3) + \frac{25}{9}\zeta(5)\right) n_f \\ &\quad + \left(\frac{151}{162} - \frac{19}{27}\zeta(3)\right) n_f^2 \\ &\quad - \frac{\pi^2}{432}(33 - 2n_f)^2 + \eta \left(\frac{55}{72} - \frac{5}{3}\zeta(3)\right) \\ &\simeq -6.637 - 1.200 n_f - 0.005 n_f^2 - 1.240\eta, \end{aligned} \tag{3.18}$$

where $\eta = (\sum_q Q_q)^2 / 3 \sum_q Q_q^2$ and the sum extends over the (n_f) quarks which are effectively massless at the energy scale $\sqrt{s}$. The Riemann ζ function,

$$\zeta(s) = \sum_{k=1}^{\infty} \frac{1}{k^s} , \tag{3.19}$$

has the values $\zeta(3) = 1.202\,057$, $\zeta(5) = 1.036\,928$. The expression for C_3 is taken from ref. [4]. For massless quarks, the QCD corrections to the ratio R_Z of hadronic to leptonic Z decay widths are again the same at this order, except that η changes to [1]

$$\eta = \frac{(\sum_q V_q)^2}{3 \sum_q (V_q^2 + A_q^2)} . \tag{3.20}$$

The μ^2 dependence of the coefficients C_2, C_3 ... is fixed by the requirement that order-by-order, the series should be independent of the choice of scale:

$$C_2\left(\frac{s}{\mu^2}\right) = C_2(1) - \pi b \ln \frac{s}{\mu^2}$$

[1] This result assumes complete isodoublets of massless quarks, see Section 3.2.

Downloaded from https://www.cambridge.org/core. UNIVERSIDAD AUTONOMA METROPOLITANA, on 15 Nov 2026 at 06:22:37, subject to the Cambridge Core terms of use, available at https://www.cambridge.org/core/terms. https://doi.org/10.1017/CBO9780511628788.004

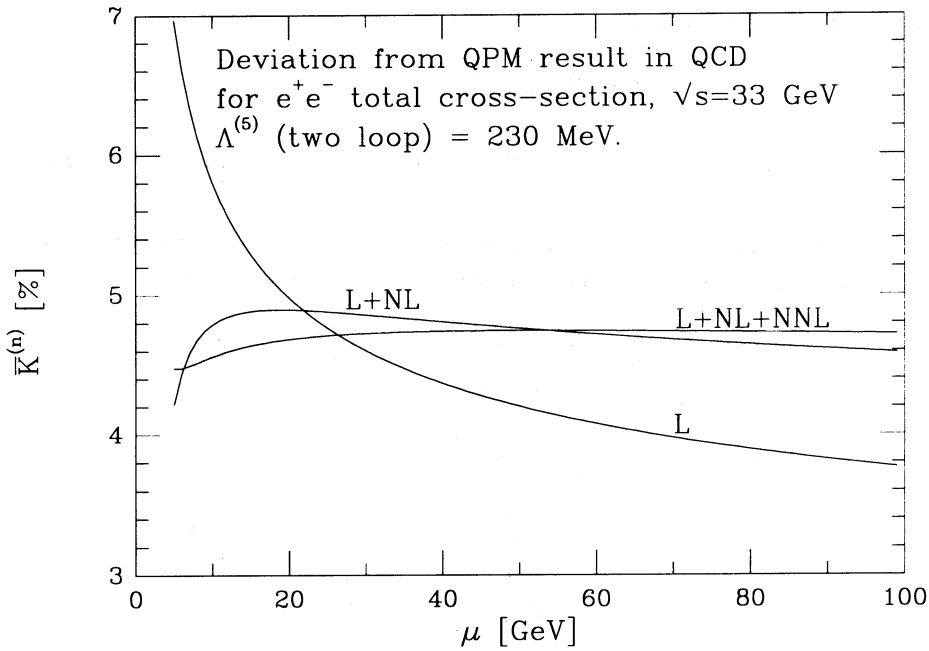


Fig. 3.3. The quantity $\overline{K}^{(n)} = K^{(n)} - 1$, where $K^{(n)}$ denotes the QCD prediction for K_{QCD} truncated at $O(\alpha_S^n)$, as a function of the renormalization scale μ.

$$C_3\left(\frac{s}{\mu^2}\right) = C_3(1) + C_1(1)\left(\pi b \ln\frac{s}{\mu^2}\right)^2 - (\pi b' + 2C_2(1))\,\pi b \ln\frac{s}{\mu^2}\,, \tag{3.21}$$

where b and b' are defined in Eq. (2.8). The above result provides an explicit example of how the coefficients of any QCD perturbative expansion depend on the choice made for the renormalization scale μ, in such a way that as μ is varied, the change in the coefficients exactly compensates the change in the coupling $\alpha_S(\mu^2)$. However this μ-independence breaks down whenever the series is *truncated*. One can show by differentiating the above expression for K_{QCD} with respect to μ that the result is $O(\alpha_S^4)$. More generally, changing the scale in a physical quantity which has been calculated to $O(\alpha_S^n)$ induces changes which are $O(\alpha_S^{n+1})$. This is illustrated in Fig. 3.3, which shows K_{QCD} defined in Eq. (3.17) as a function of μ, as the higher-order terms are added in. As expected, the more terms are added, the more stable the prediction.

In the absence of higher-order corrections, one can try to guess the 'best' choice of scale (more generally, renormalization scheme), defined as

Downloaded from https://www.cambridge.org/core. UNIVERSIDAD AUTONOMA METROPOLITANA, on 15 Nov 2026 at 06:22:37, subject to the Cambridge Core terms of use, available at https://www.cambridge.org/core/terms. https://doi.org/10.1017/CBO9780511628788.004

the scale which makes the truncated and all-orders predictions equal.[2] In the literature, various particular choices have been advocated. Suppose that the perturbation series for R has been calculated to order α_S^n. In the *fastest apparent convergence* (FAC) approach, one chooses the scale $\mu = \mu_{FAC}$, where

$$R^{(1)}(\mu_{FAC}) = R^{(n)}(\mu_{FAC}). \tag{3.22}$$

On the other hand, the *principle of minimal sensitivity* (PMS) [5] imposes the known renormalization-scheme independence of the all-orders result on the truncated calculation. Within the $\overline{\rm MS}$ renormalization prescription, this suggests a scale choice $\mu = \mu_{PMS}$, where

$$\mu \frac{d}{d\mu} R^{(n)}(\mu)\Big|_{\mu_{PMS}} = 0\,. \tag{3.23}$$

A third approach (BLM [6]) argues that the n_f dependent terms in the coefficients indicate which parts should be associated with the the QCD β function, and that the appropriate scale is the one which absorbs all these terms into α_S. To $O(\alpha_S^2)$, it is straightforward to calculate these three special scales from Eq. (3.21):

$$\begin{aligned}
\mu_{FAC} &= \sqrt{s}\exp\left(-\frac{C_2(1)}{2\pi b}\right) \simeq 0.692\sqrt{s}\,, \\
\mu_{PMS} &= \sqrt{s}\exp\left(-\frac{\pi b' + 2C_2(1)}{4\pi b}\right) \simeq 0.587\sqrt{s}\,, \\
\mu_{BLM} &= \sqrt{s}\exp\left(2\zeta(3) - \frac{11}{4}\right) \simeq 0.708\sqrt{s}\,,
\end{aligned} \tag{3.24}$$

where $C_2(1)$ is given in Eq. (3.18) and five massless flavours have been assumed. In the present context, these three scales are numerically rather close (the first two can be identified directly in Fig. 3.3), indicating that the scale dependence of R is rather weak, and that the α_S value obtained from fitting the above expressions to the e^+e^- total cross section or the Z hadronic decay width should be reliable. The results of such fits will be discussed in Chapter 12. It is, however, important to remember that there are no theorems that *prove* that any of the above scale-fixing schemes are correct. All one can say is that the theoretical error on a quantity calculated to $O(\alpha_S^n)$ is always $O(\alpha_S^{n+1})$. Fixing a special scale does *not* remove this theoretical error on the prediction. One can vary the scale over some 'physically reasonable range' (for example, the range of momentum scales flowing through the Feynman diagrams) to try to quantify this uncer-

[2] We do not address here the meaning of an 'all-orders' summation of what is an asymptotic rather than a convergent series.

Downloaded from https://www.cambridge.org/core. UNIVERSIDAD AUTONOMA METROPOLITANA, on 15 Nov 2026 at 06:22:37, subject to the Cambridge Core terms of use, available at https://www.cambridge.org/core/terms. https://doi.org/10.1017/CBO9780511628788.004

tainty, but ultimately there is no substitute for actually performing the higher-order calculations.

3.2 Heavy quark production

The results presented in the previous section for the cross sections for $e^+e^- \to q\bar{q}, q\bar{q}g, \ldots$ are valid only for massless quarks, $m_q = 0$. This is a reasonable approximation for the u, d, s and c quarks at high-energy colliders such as LEP and SLC. For b and t quarks, however, the expressions must be modified to take the non-negligible quark mass into account. In this section we present some basic results for massive quarks. We use the notation Q for the field of a heavy quark of mass m.

We begin with the lowest-order process, $e^+e^- \to Q\overline{Q}$. There are two sources of mass effects — the matrix element and the phase space integration. Energy conservation embodied in the latter causes the cross section to vanish for $\sqrt{s} \leq 2m$.[3] It is convenient to introduce the quark *velocity*

$$\beta = \sqrt{1 - \frac{4m^2}{s}}\,, \tag{3.25}$$

so that $\beta = 0$ corresponds to the heavy quark threshold, and the results for massless quarks are recovered in the relativistic limit $\beta \to 1$.

A straightforward calculation gives the analogues of Eqs. (3.7,3.8) for massive quarks,

$$\begin{aligned} R(\beta) &= 3Q_Q^2 \beta \frac{3-\beta^2}{2} \\ R_Z(\beta) &= \frac{3\beta}{A_\mu^2 + V_\mu^2}\left(\beta^2 A_Q^2 + \frac{3-\beta^2}{2} V_Q^2\right) \\ &\equiv R_{ZA}(\beta) + R_{ZV}(\beta)\,. \end{aligned} \tag{3.26}$$

Notice that the dependence on the mass is *different* for the vector and axial-vector parts of R_Z, since the quark mass breaks chiral invariance. For the same reason, the higher-order QCD corrections are also different:[4]

$$\begin{aligned} R_Z(\beta) &= R_{ZV}(\beta)\left[1 + c_1\frac{\alpha_S}{\pi} + c_2\left(\frac{\alpha_S}{\pi}\right)^2 + \ldots\right] \\ &+ R_{ZA}(\beta)\left[1 + d_1\frac{\alpha_S}{\pi} + d_2\left(\frac{\alpha_S}{\pi}\right)^2 + \ldots\right]\,. \end{aligned} \tag{3.27}$$

[3] We shall consider only the idealized case of *stable* heavy quarks. Otherwise the behaviour near threshold is influenced by finite decay width effects.

[4] We use the notation of ref. [7].

Downloaded from https://www.cambridge.org/core. UNIVERSIDAD AUTONOMA METROPOLITANA, on 15 Nov 2026 at 06:22:37, subject to the Cambridge Core terms of use, available at https://www.cambridge.org/core/terms. https://doi.org/10.1017/CBO9780511628788.004

The higher-order coefficients contain logarithms of s/m^2 which originate in the running of the quark mass, as described in Section 2.4. These can be removed by replacing the 'bare' mass m by the running mass $m(s)$ in, say, the $\overline{\text{MS}}$ renormalization scheme.

The $O(\alpha_S)$ correction coefficients c_1 and d_1 are known for arbitrary quark mass [8], but the expressions are too unwieldy to present here. For small quark masses, a good approximation is [7]

$$\begin{aligned} c_1 &= 1 + 12\epsilon + \ldots \\ d_1 &= 1 - 22\epsilon + \ldots , \end{aligned} \tag{3.28}$$

where $\epsilon = m^2(s)/s \ll 1$. Note that setting $\epsilon = 0$ reproduces the massless quark results $c_1 = d_1 = 1$. The coefficients c_2 and d_2 are also known in the small-quark-mass approximation [9]:

$$\begin{aligned} c_2 &= 1.4092 + 104.83\epsilon + \ldots \\ d_2 &= 1.4092 - 85.72\epsilon + \ldots \end{aligned} \tag{3.29}$$

in the $\overline{\text{MS}}$ scheme with $n_f = 5$ and $\alpha_S = \alpha_S(s)$ in (3.27). In e^+e^- annihilation at the Z pole the precision of the R_Z measurement is such that the effects due to the finite b quark mass ($\epsilon \approx 10^{-3}$) must be taken into account in the coefficients to $O(\alpha_S^2)$.

The result for d_2 in Eq. (3.29) is strictly only valid for mass-degenerate weak isospin quark doublets. When the mass difference between the quarks in the same doublet becomes large, there is an additional large contribution. This is related to the triangle anomaly for axial currents. In particular, for $m_t > M_Z \gg m_b$ [10],

$$\delta d_2 \approx \ln\left(\frac{M_Z^2}{m_t^2}\right) - \frac{37}{12} + O\left(\frac{M_Z^2}{m_t^2}\right) . \tag{3.30}$$

3.3 Jet cross sections

The expression given for the total hadronic cross section in Section 3.1 is very concise, but it tells us nothing about the kinematic *distribution* of hadrons in the final state. If the hadronic fragments of a fast moving quark have limited transverse momentum relative to the quark momentum (collinear fragmentation), then the lowest-order contribution to the cross section, $e^+e^- \to q\bar{q}$, can naively be interpreted as the production of two back-to-back jets. Experimentally, it *does* appear to be true that most events are 'two-jet-like', with a smaller fraction containing three jets, an even smaller fraction containing four jets, and so on. At first sight, this seems consistent with our intuition that each jet after the first two should correspond to the emission of a gluon off the quark lines, each emission

Downloaded from https://www.cambridge.org/core. UNIVERSIDAD AUTONOMA METROPOLITANA, on 15 Nov 2026 at 06:22:37, subject to the Cambridge Core terms of use, available at https://www.cambridge.org/core/terms. https://doi.org/10.1017/CBO9780511628788.004

'costing' a power of $\alpha_S \ll 1$. However, this simple picture, although essentially correct, masks a much more complicated situation, which involves both perturbative and non-perturbative aspects of the theory. In this section we will attempt to construct a theory of jets based on the lowest orders in perturbation theory. In subsequent chapters, we will extend this to higher orders and describe how to include the non-perturbative transition from a final state involving quarks and gluons to one involving the hadrons which are measured by experiment.

We begin by considering the next-to-leading process $e^+e^- \to q\bar{q}g$. From the previous section (Eq. (3.11)), we have

$$\frac{1}{\sigma}\frac{d^2\sigma}{dx_1 dx_2} = C_F\frac{\alpha_S}{2\pi}\frac{x_1^2+x_2^2}{(1-x_1)(1-x_2)}\,. \tag{3.31}$$

Recall that this cross section becomes (infinitely) large when one or both of the x_i approach 1, which corresponds to the gluon being collinear with one of the quarks, or soft (*i.e.* its energy is small compared to $\sqrt{s}$) respectively. If we again assume that quarks and gluons fragment collinearly into hadrons, then this preference for the gluon to be soft or collinear means that the two-jet-like structure of the lowest order is maintained at $O(\alpha_S)$. If, on the other hand, the gluon is *required* to be well-separated in phase space from the quarks — a configuration which we might identify as a 'three-jet event' — then the singular regions of the matrix element are avoided and the cross section is suppressed relative to lowest order by one power of α_S. In fact, this qualitative result holds to *all* orders of perturbation theory. The amplitudes for multiple gluon emission contain the same type of singularities as those which appear at first order, which leads to a final state which is predominantly 'two-jet-like', with a smaller probability (determined by α_S) for three or more distinguishable jets.

To make all this more quantitative, we need to introduce the concept of a *jet measure*, *i.e.* a procedure for classifying a final state of hadrons (experimentally) or quarks and gluons (theoretically) according to the number of jets it contains. To be useful, a jet measure should give cross sections which, like the total cross section, are free of soft and collinear singularities when calculated in perturbation theory, and should also be relatively insensitive to the non-perturbative fragmentation of quarks and gluons into hadrons.

One of the first attempts to define jet cross sections in perturbation theory was by Sterman and Weinberg [11]. In their picture, a final state is classified as two-jet-like if all but a fraction ϵ of the total available energy is contained in a pair of cones of half-angle δ. The two-jet cross section is then obtained by integrating the matrix elements for the various quark and gluon final states over the appropriate region of phase space determined by ϵ and δ. At lowest order, the two-jet and total cross sections

Downloaded from https://www.cambridge.org/core. UNIVERSIDAD AUTONOMA METROPOLITANA, on 15 Nov 2026 at 06:22:37, subject to the Cambridge Core terms of use, available at https://www.cambridge.org/core/terms. https://doi.org/10.1017/CBO9780511628788.004

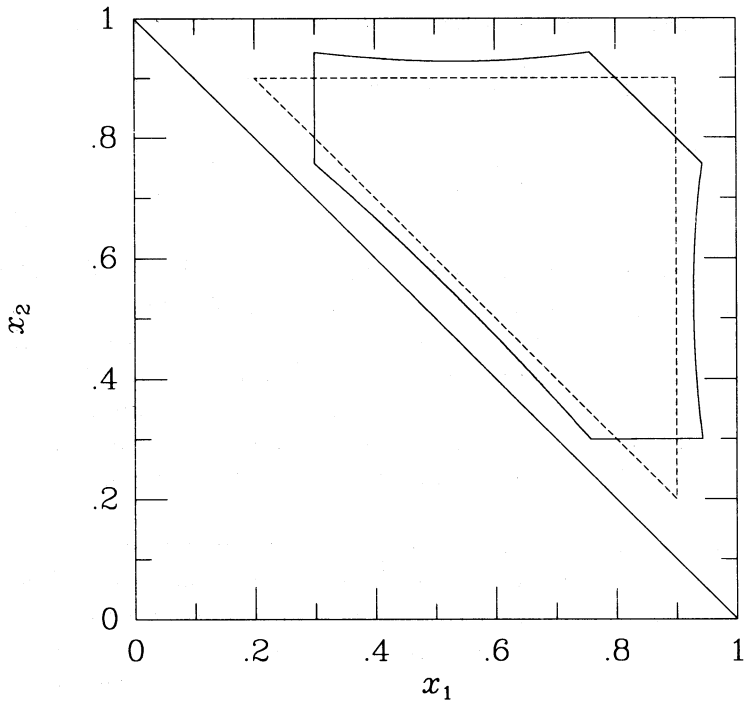


Fig. 3.4. Boundaries between the two- and three-jet regions in the (x_1, x_2) plane for Sterman-Weinberg jets with $(\epsilon, \delta) = (0.3, 30°)$ (solid lines), and JADE algorithm jets with $y = 0.1$ (dashed lines).

obviously coincide, for any values of the parameters. At $O(\alpha_S)$, the two-jet cross section is obtained by integrating the right-hand side of Eq. (3.31) over the appropriate range of x_1 and x_2. Fig. 3.4 shows the boundaries (solid lines) for the specific choice of parameters $\epsilon = 0.3$ and $\delta = 30°$. The two-jet region is the narrow band between these boundaries and the edges of the triangle. Note that the δ constraint corresponds to the curved portions of the boundary, while the ϵ constraint gives the straight line segments at the corners.

Rather than calculating the two-jet cross section directly, integrating the $q\bar{q}g$ matrix element (in n dimensions) over this region and adding the contribution from the virtual gluon diagrams, it is easier to use the fact that at this order $\sigma = \sigma_2 + \sigma_3$. The two-jet cross section can therefore be obtained by subtracting the three-jet cross section from the total cross section already obtained in Section 3.1. The advantage of this is that the calculation of σ_3 can be performed in four dimensions, since the matrix element singularities are outside the three-jet region at this order. Defining

Downloaded from https://www.cambridge.org/core. UNIVERSIDAD AUTONOMA METROPOLITANA, on 15 Nov 2026 at 06:22:37, subject to the Cambridge Core terms of use, available at https://www.cambridge.org/core/terms. https://doi.org/10.1017/CBO9780511628788.004

the two- and three-jet fractions by $f_i = \sigma_i/\sigma$ $(i = 2, 3)$ we obtain[5]

$$\begin{aligned} f_2 &= 1 - 8C_F\frac{\alpha_S}{2\pi}\left\{\ln\frac{1}{\delta}\left[\ln\left(\frac{1}{2\epsilon}-1\right)-\frac{3}{4}+3\epsilon\right]\right. \\ &\qquad \left. +\frac{\pi^2}{12}-\frac{7}{16}-\epsilon+\frac{3}{2}\epsilon^2+O(\delta^2\ln\epsilon)\right\}, \\ f_3 &= 1 - f_2\,. \end{aligned} \tag{3.32}$$

Notice that when the parameters ϵ and δ are small, the $O(\alpha_S)$ correction becomes logarithmically large. This is simply the vestige of the soft and collinear singularities. We shall discuss in Chapter 6 techniques for resumming terms analogous to the $\alpha_S \ln\delta$ terms in Eq. (3.32) to all orders in perturbation theory; when δ is small this should improve on the first-order result. On the other hand, as the parameters become large, the three-jet region in Fig. 3.4 shrinks and the three-jet fraction decreases, as expected.

At higher orders in perturbation theory, we can have events with more than three jets. For example, the $O(\alpha_S^2)$ $q\bar{q}q\bar{q}$ and $q\bar{q}gg$ production processes can give rise to two, three or four jet events, depending on the separation in phase space and energy of the outgoing partons. It turns out that from an experimental and theoretical point of view, the Sterman-Weinberg jet definition based on cones is not well-suited to analysing multijet final states. One of the reasons is that fixed-angle cones give an inefficient 'tiling' of the phase space 4π solid angle. For this reason, various alternatives have been proposed, the most important of which is the 'minimum invariant mass' or JADE algorithm [12], which we shall now describe.

Consider $q\bar{q}g$ production at $O(\alpha_S)$, *i.e.* with three partons in the final state. A three-jet event is defined as one in which the minimum invariant mass of the parton pairs is larger than some fixed fraction y (sometimes called y_{cut}) of the overall centre-of-mass energy:

$$\min\,(p_i+p_j)^2 = \min\,2E_iE_j(1-\cos\theta_{ij}) > ys, \qquad i,j = q,\bar{q},g\,, \tag{3.33}$$

for massless partons in the e^+e^- centre-of-mass frame. It is easily shown that this region of phase space avoids the soft and collinear singularities of the matrix element. In fact in terms of the energy fractions, Eq. (3.33) is equivalent to

$$0 < x_1, x_2 < 1-y, \qquad x_1+x_2 > 1+y \quad \left(y \le \tfrac{1}{3}\right)\,. \tag{3.34}$$

The corresponding boundary (for $y = 0.1$) is shown by the dashed lines in Fig. 3.4. Just as for the Sterman-Weinberg jets, the two- and three-

[5] We show here only those terms which are important when δ is small. The full expression is rather unwieldy.

Downloaded from https://www.cambridge.org/core. UNIVERSIDAD AUTONOMA METROPOLITANA, on 15 Nov 2026 at 06:22:37, subject to the Cambridge Core terms of use, available at https://www.cambridge.org/core/terms. https://doi.org/10.1017/CBO9780511628788.004

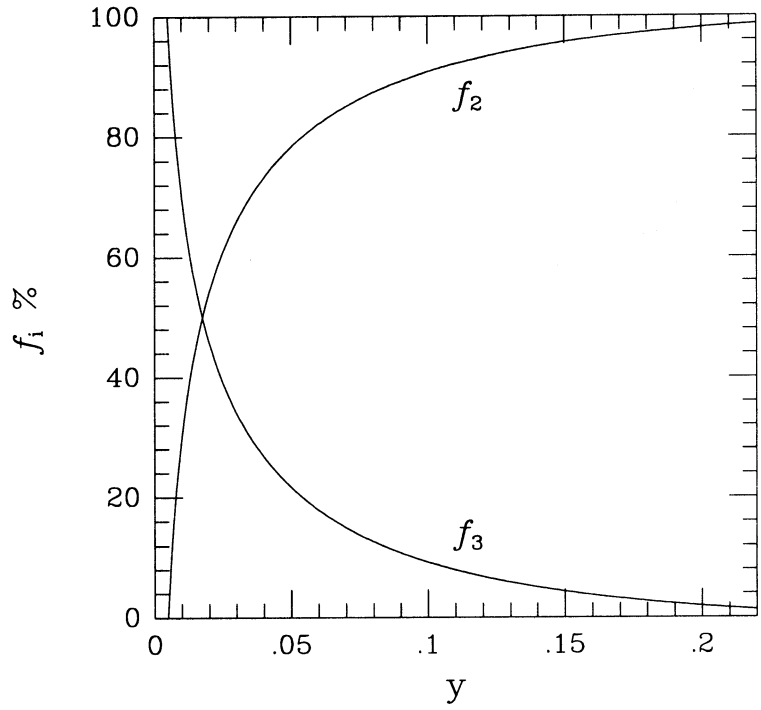


Fig. 3.5. The functions f_2 and f_3 from Eq. (3.35).

jet fractions to $O(\alpha_S)$ are obtained by integrating the right-hand side of Eq. (3.11) over the appropriate region:

$$\begin{aligned} f_3 &= C_F \frac{\alpha_S}{2\pi} \left[(3-6y) \ln\left(\frac{y}{1-2y}\right) + 2\ln^2\left(\frac{y}{1-y}\right) \right. \\ &\quad \left. + \frac{5}{2} - 6y - \frac{9}{2}y^2 + 4\,\mathrm{Li}_2\left(\frac{y}{1-y}\right) - \frac{\pi^2}{3} \right] , \\ f_2 &= 1 - f_3 , \end{aligned} \tag{3.35}$$

where Li_2 is the dilogarithm function,

$$\begin{aligned} \mathrm{Li}_2(x) &= -\int_0^x dy\, \frac{\ln(1-y)}{y} \\ &= \frac{x}{1^2} + \frac{x^2}{2^2} + \frac{x^3}{3^2} + \ldots \text{ for } |x| \leq 1 . \end{aligned} \tag{3.36}$$

The soft and collinear singularities again appear as large logarithms in the limit $y \to 0$. Clearly the result in Eq. (3.35) only makes sense for y values large enough such that $f_2 \gg f_3$, so that the $O(\alpha_S)$ correction to f_2 is perturbatively small. Fig. 3.5 shows the functions $f_2(y)$ and $f_3(y)$ from Eq. (3.35) for $\alpha_S = 0.118$.

Downloaded from https://www.cambridge.org/core. UNIVERSIDAD AUTONOMA METROPOLITANA, on 15 Nov 2026 at 06:22:37, subject to the Cambridge Core terms of use, available at https://www.cambridge.org/core/terms. https://doi.org/10.1017/CBO9780511628788.004

The generalization to multijet fractions is straightforward, using the following algorithm. Starting from an n-parton final state, identify the pair with the minimum invariant mass squared. If this is greater than ys then the number of jets is n. If not, combine the minimum pair into a single 'cluster'. Then repeat for the $(n-1)$-parton/cluster final state, and so on until all partons/clusters have a relative invariant mass squared greater than ys. The number of clusters remaining is then the number of jets in the final state. According to this definition, an n-parton final state can give any number of jets between n (all partons well-separated) and 2 (for example, two energetic quarks accompanied by soft and collinear gluons).

Since a soft or collinear gluon emitted from a quark line does not change the multiplicity of jets, the cancellation of the corresponding singularities that was evident in the total cross section calculation can still take place, and the jet fractions defined this way are 'infra-red safe', *i.e.* free of such singularities to all orders in perturbation theory. We shall discuss other examples of infra-red safe jet variables below.

Now in general we have

$$f_{n+2}(\sqrt{s},y) = \left(\frac{\alpha_S(\mu^2)}{2\pi}\right)^n \sum_{j=0}^{\infty} C_{nj}\left(y,\frac{s}{\mu^2}\right)\left(\frac{\alpha_S(\mu^2)}{2\pi}\right)^j, \quad n \geq 0,$$

$$\sum_{n=2}^{\infty} f_n = 1\,. \tag{3.37}$$

We follow the convention in the literature of expanding the perturbation series for the total cross section and jet cross sections in powers of (α_S/π) and $(\alpha_S/2\pi)$ respectively. In (3.37) we have assumed some particular renormalization prescription ($\overline{\rm MS}$ is almost always used in practice) and introduced μ as the renormalization scale. Since the jet parameter y is dimensionless, with the choice $\mu = \sqrt{s}$ all the energy dependence of the jet fractions is contained in the coupling $\alpha_S(s)$. One can therefore exhibit, at least in principle, the *running* of the strong coupling by measuring, for example, a decrease in f_3 as $\sqrt{s}$ increases, see Fig. 3.6.

In experiments, the JADE algorithm is applied to final-state *hadrons* rather than *partons*.[6] However studies using hadronization models to describe the transition from partons to hadrons have shown that — at least at high energy — the hadronization corrections are small and therefore the QCD parton-level predictions can be reliably compared with the experimental data. This will be discussed further in Chapter 5.

The next-to-leading-order corrections to f_3 have been calculated [14].

[6] There are in fact several slight variants of the JADE algorithm which are used in practice, see ref. [13].

Downloaded from https://www.cambridge.org/core. UNIVERSIDAD AUTONOMA METROPOLITANA, on 15 Nov 2026 at 06:22:37, subject to the Cambridge Core terms of use, available at https://www.cambridge.org/core/terms. https://doi.org/10.1017/CBO9780511628788.004

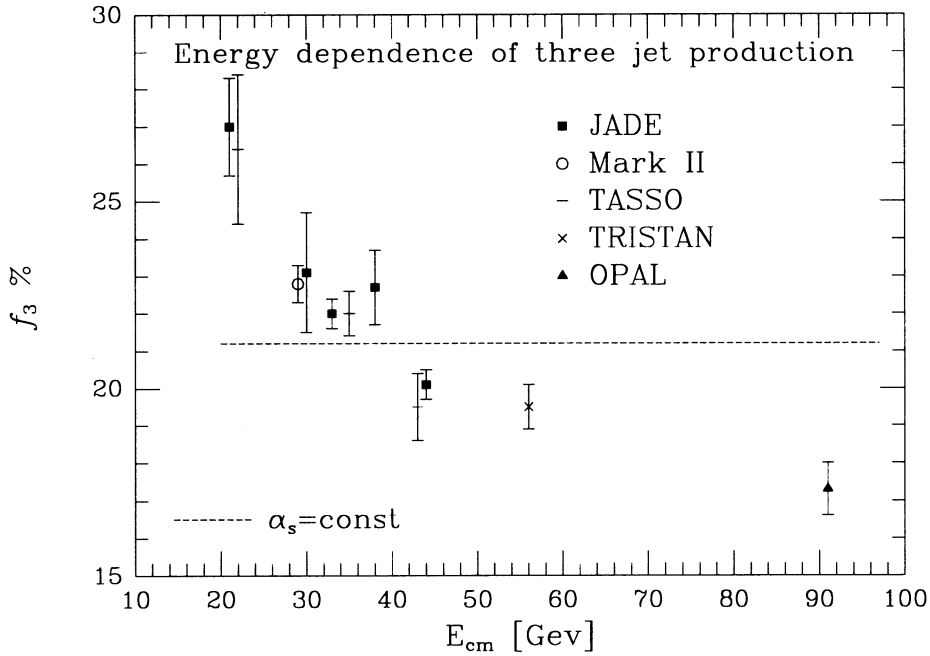


Fig. 3.6. A compilation of three-jet fractions at different e^+e^- annihilation energies. Adapted from ref. [15].

Because the hadronization corrections to f_3 are small, the three-jet rate provides one of the most precise measurements of α_S at e^+e^- colliders. A typical fit is shown in Fig. 3.7 [15]. The curves correspond to the perturbative predictions calculated in the $\overline{\text{MS}}$ prescription with two different choices of scale. At large y, the events are mostly classified as two (broad) jets. As y decreases, and the jets are allowed to be narrower, fewer events are two-jet and the number of multijet events increases. Notice that at medium and large y, where these calculations should be most reliable, both scale choices give equally acceptable fits, *but with different values of* $\Lambda_{\overline{\text{MS}}}$. This is an example of the scale-dependence uncertainty discussed above. At smaller y, there appears to be some preference for the curve corresponding to the smaller scale. However, some care must be taken with this interpretation. We have already seen (Eq. (3.35)) that when y is so small that $\alpha_S \ln^2 y \sim 1$, the perturbation series for f_2 breaks down. In fact one can show that all the jet fractions have higher-order corrections which contain terms like $\alpha_S^n \ln^{2n} y$ at small y. Before concluding anything about which renormalization scales are 'preferred', we should make sure that these large corrections are correctly taken into account. We shall see in Chapter 6 that when this is done, there is no longer any preference in the data for a small scale, and indeed the overall scale-dependence

Downloaded from https://www.cambridge.org/core. UNIVERSIDAD AUTONOMA METROPOLITANA, on 15 Nov 2026 at 06:22:37, subject to the Cambridge Core terms of use, available at https://www.cambridge.org/core/terms. https://doi.org/10.1017/CBO9780511628788.004

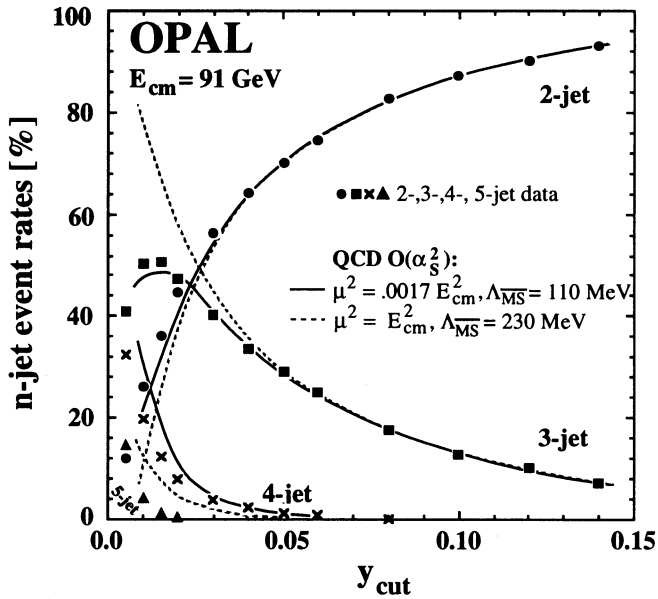


Fig. 3.7. QCD fits to the jet rates at LEP, as measured by the OPAL collaboration. Figure from ref. [15].

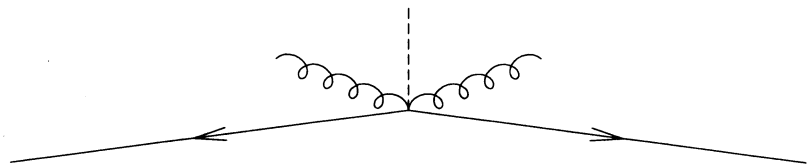


Fig. 3.8. An example of a configuration which the JADE algorithm classifies as a three-jet event.

uncertainty in the extracted value of the coupling is reduced.

While the JADE algorithm is well suited to experimental jet measurements, it is not quite optimal from a theoretical point of view. We have already remarked that when y is small, the $O(\alpha_S^n \ln^{2n} y)$ terms must be resummed to all orders to obtain a reliable prediction. Unfortunately, the algorithm is not readily amenable to this type of resummation [16]. This reflects a tendency for the algorithm to reconstruct 'spurious' jets, *i.e.* clusters of hadrons or partons whose net momentum does not obviously coincide with any approximately collinear set of particles in the actual event. An example is provided by the configuration shown in Fig. 3.8, where two soft gluons are emitted close to the quark and antiquark. Even though the two gluons have a large relative angle, their invariant mass is the smallest in the event. If this is smaller than y, the algorithm combines

Downloaded from https://www.cambridge.org/core. UNIVERSIDAD AUTONOMA METROPOLITANA, on 15 Nov 2026 at 06:22:37, subject to the Cambridge Core terms of use, available at https://www.cambridge.org/core/terms. https://doi.org/10.1017/CBO9780511628788.004

them into a single cluster, whose direction is indicated by the dashed line in the figure. If after this clustering all remaining invariant masses exceed the critical value determined by y, the event is classified as three jet, even though the direction of the third 'cluster' jet does not coincide with any of the original partons in the event.

To overcome these problems, a variant of the JADE algorithm — the k_T or 'Durham' algorithm — has been proposed [17]. In this new algorithm, the invariant mass measure of two partons (hadrons), defined in Eq. (3.33), is replaced by a quantity which, when the angle between the partons is small, is the minimum of the relative transverse momenta:

$$2 \min(E_i^2, E_j^2)\,(1 - \cos\theta_{ij}) > ys, \tag{3.38}$$

in the e^+e^- centre-of-mass frame. Notice that with this new definition, the configuration in Fig. 3.8 is classified, more naturally, as a two-jet event, since the relative transverse momentum of the gluons is larger than that of the two pairs of quarks and gluons. Using this modified algorithm, the jet fractions can be calculated in perturbation theory as before. At $O(\alpha_S)$, the conditions for two- and three-jet events implied by Eq. (3.38) again define a boundary in the (x_1, x_2) plane. Analogous expressions for f_2 and f_3 to those in Eq. (3.35) can then be obtained. As we shall see in Chapter 6, with this new definition of the jet measure resummation of the large logarithms can be performed [17], and the range of applicability can be extended to smaller values of y where comparison with data can be made. The next-to-leading-order corrections for the k_T algorithm have also been calculated [13] and comparisons of theory and experiment have been performed, as for the JADE algorithm. The corresponding α_S values for the various algorithms, with and without resummation, will be presented in Chapter 12.

3.4 Event shape variables

Another approach to studying the jet-like characteristics of hadronic final states in e^+e^- annihilation is to use 'shape variables'. The idea is to define a quantity which characterizes the 'shape' of an event, for example whether the distribution of hadrons is pencil-like, planar, spherical etc. This is more general than the jet cross section approach discussed above, since a jet-finding algorithm will *always* find jets in a hadronic final state even when none existed in the first place, for example in the limiting case when the hadronic energy is distributed uniformly over the 4π solid angle.

The procedure, then, is to define a quantity X which measures some particular aspect of the shape of the hadronic final states. The distribution $d\sigma/dX$ can be measured and compared with the theoretical predic-

Downloaded from https://www.cambridge.org/core. UNIVERSIDAD AUTONOMA METROPOLITANA, on 15 Nov 2026 at 06:22:37, subject to the Cambridge Core terms of use, available at https://www.cambridge.org/core/terms. https://doi.org/10.1017/CBO9780511628788.004

tion. For the latter to be calculable in perturbation theory, the variable should be infra-red safe, *i.e.* insensitive to the emission of soft or collinear gluons. In particular, if $\boldsymbol{p}_i$ is any momentum[7] occurring in its definition, it must be invariant under the branching

$$\boldsymbol{p}_i \to \boldsymbol{p}_j + \boldsymbol{p}_k \tag{3.39}$$

whenever $\boldsymbol{p}_j$ and $\boldsymbol{p}_k$ are parallel or one of them is small. Quantities made out of *linear* sums of momenta meet this requirement. Some widely-used examples are

(i) thrust [18]

$$T = \max_{\boldsymbol{n}} \frac{\sum_i |\boldsymbol{p}_i \cdot \boldsymbol{n}|}{\sum_i |\boldsymbol{p}_i|} \tag{3.40}$$

(ii) spherocity [19]

$$S = \left(\frac{4}{\pi}\right)^2 \min_{\boldsymbol{n}} \left(\frac{\sum_i |\boldsymbol{p}_i \times \boldsymbol{n}|}{\sum_i |\boldsymbol{p}_i|}\right)^2 \tag{3.41}$$

(iii) C-parameter [20]

$$C = \frac{3}{2} \frac{\sum_{i,j} [|\boldsymbol{p}_i|\,|\boldsymbol{p}_j| - (\boldsymbol{p}_i \cdot \boldsymbol{p}_j)^2/|\boldsymbol{p}_i|\,|\boldsymbol{p}_j|]}{(\sum_i |\boldsymbol{p}_i|)^2} \,. \tag{3.42}$$

In these definitions, $\boldsymbol{p}_i$ are the final-state hadron (or parton) momenta and $\boldsymbol{n}$ is an arbitrary unit vector. If the $\boldsymbol{p}_i$ form an almost collinear jet, then after the specified maximization or minimization $\boldsymbol{n}$ will lie along the jet in the case of T or S (defining the thrust or spherocity axes, respectively). The values of the above shape variables for the idealized cases of perfectly pencil-like and spherical events are given in Table 3.1.

At lowest order in perturbation theory, $e^+e^- \to q\bar{q}$, the event shape variables have the values listed in the first row in Table 3.1. At $O(\alpha_S)$, the distribution in the the shape variable $d\sigma/dX$ ($X = T, S, \ldots$) is obtained by integrating the right-hand side of Eq. (3.11) over x_1 and x_2 with the constraint

$$\delta(X - f_X(x_1, x_2, x_3 = 2 - x_1 - x_2)) \,, \tag{3.43}$$

i.e. along a contour in the (x_1, x_2) plane. The functions f_X are listed in the third row in Table 3.1. Note that as long as the variables are not

[7] Boldface quantities denote three-momenta.

Downloaded from https://www.cambridge.org/core. UNIVERSIDAD AUTONOMA METROPOLITANA, on 15 Nov 2026 at 06:22:37, subject to the Cambridge Core terms of use, available at https://www.cambridge.org/core/terms. https://doi.org/10.1017/CBO9780511628788.004

Quantity	T	S	C
pencil-like event	1	0	0
spherical event	$\frac{1}{2}$	1	1
$q\bar{q}g$	$\max\{x_i\}$	$\frac{16}{\pi^2}\frac{\prod_i (1-x_i)}{\max\{x_i^2\}}$	$6\,\frac{\prod_i (1-x_i)}{x_1 x_2 x_3}$

Table 3.1. Values of the shape variables for different event types. The third row gives the constraint functions f_X of Eq. (3.43).

equal to their pencil-like limits, *e.g.* $T < 1$, then these distributions are finite, since the soft and collinear configurations are excluded from the integration range.

For the thrust distribution, the function f_T gives exactly the same integration contour as the two-jet/three-jet boundary for the JADE algorithm, Fig. 3.4. A straightforward calculation gives

$$\frac{1}{\sigma}\frac{d\sigma}{dT} = C_F \frac{\alpha_S}{2\pi}\left[\frac{2(3T^2-3T+2)}{T(1-T)}\ln\left(\frac{2T-1}{1-T}\right) - \frac{3(3T-2)(2-T)}{(1-T)}\right]. \tag{3.44}$$

As expected, the distribution diverges as $T \to 1$, reflecting the soft and collinear gluon singularities in the matrix element. The virtual gluon contribution at this order gives a singular contribution proportional to $\delta(T-1)$, such that (with a suitable regularization procedure) the correct result for the total cross section is obtained when $d\sigma/dT$ is integrated over $\frac{1}{2} \le T \le 1$.

The thrust distribution for $T \simeq 1$ is dominated by two-jet configurations. In fact we can use the distribution integrated over $T_0 < T < 1$ to define a two-jet measure analogous to f_2, with $1-T_0$ playing the role of y. The tail of the distribution away from $T = 1$ is, on the other hand, dominated by multijet final states. In this region we have a direct test of the QCD matrix elements, through the shape of the distribution, and also a measurement of the strong coupling α_S, through the normalization. This can be done with high precision, since the next-to-leading corrections for the $(T < 1)$ thrust distribution (and indeed the other shape variables) are known [21]. The results of such measurements will be presented in Chapter 12. Care must be taken near $T = 1$ where (a) hadronization corrections become large, and (b) terms of order $[\alpha_S \ln^2(1-T)]^n$ appear in the perturbation series. This will be discussed further in Chapter 6.

It was quantities like the thrust distribution which provided the first indications that gluons are *vector* particles. For *scalar* gluons (in the adjoint representation of SU(3)), the distribution in x_1 and x_2 for $q\bar{q}g$

Downloaded from https://www.cambridge.org/core. UNIVERSIDAD AUTONOMA METROPOLITANA, on 15 Nov 2026 at 06:22:37, subject to the Cambridge Core terms of use, available at https://www.cambridge.org/core/terms. https://doi.org/10.1017/CBO9780511628788.004

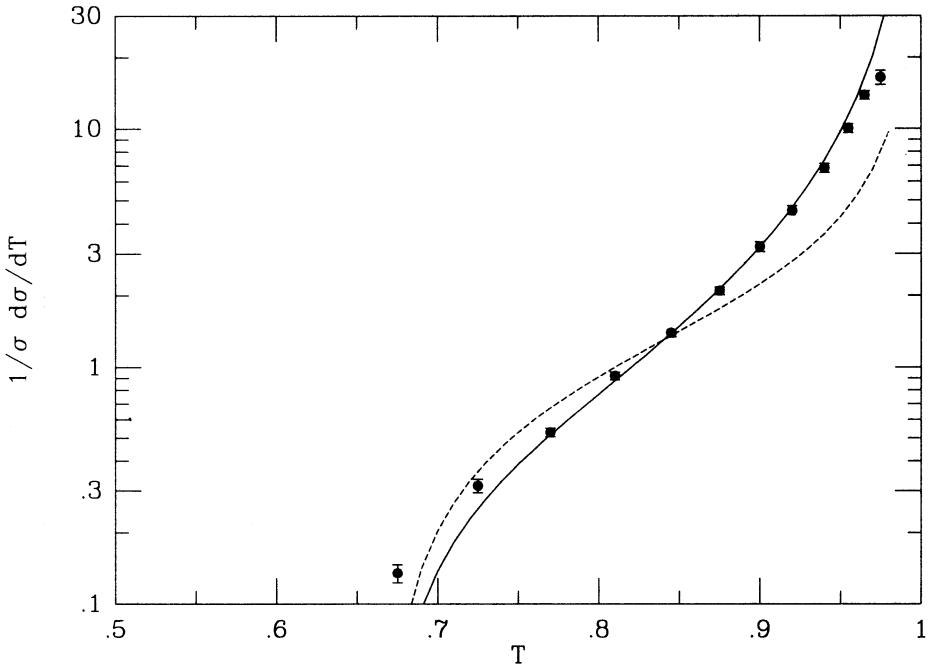


Fig. 3.9. The thrust distribution measured at LEP, showing data from the DELPHI collaboration [22] for $T < 0.98$, together with predictions of scalar gluon (dashed line) and vector gluon (solid line) theories.

production is obtained from Eq. (3.11) by the replacement

$$x_1^2 + x_2^2 \to \tfrac{1}{2}x_3^2 = \tfrac{1}{2}(2 - x_1 - x_2)^2 \tag{3.45}$$

in the numerator. Fig. 3.9 shows a comparison of data on the thrust distribution measured at LEP with the predictions of the $O(\alpha_S)$ vector and scalar gluon theories. The values of α_S (0.265 and 1.59 respectively) are chosen to give the best fit to the distribution away from $T = 1$. The scalar gluon theory is evidently ruled out. Note the slight discrepancy between the vector gluon prediction and the data at both large and small T. For the former, this is precisely the region where higher-order, logarithmic contributions become important. At small T, on the other hand, contributions from higher-order multiparton production are important. In fact a more complete calculation, with resummation of large logarithms and higher-order contributions included, gives good agreement over the whole range, see Fig. 6.12.

Finally, we mention briefly the *energy-energy correlation function* (EEC) [23], another quantity which is related to the shape variables already discussed and which is also widely used to test QCD at e^+e^- colliders. The

Downloaded from https://www.cambridge.org/core. UNIVERSIDAD AUTONOMA METROPOLITANA, on 15 Nov 2026 at 06:22:37, subject to the Cambridge Core terms of use, available at https://www.cambridge.org/core/terms. https://doi.org/10.1017/CBO9780511628788.004

EEC is a dimensionless angular distribution defined by

$$\frac{1}{\sigma}\frac{d\Sigma}{d\cos\chi} = \sum_{\substack{i,j \\ i\neq j}} \int \frac{d^3p_i}{E_i}\frac{d^3p_j}{E_j}\left(\frac{2E_iE_j}{s}\right)E_iE_j\frac{d^6\sigma}{d^3p_id^3p_j}\delta(\hat{n}_i.\hat{n}_j - \cos\chi)$$
$$+\sum_i \int \frac{d^3p_i}{E_i}\left(\frac{E_i^2}{s}\right)E_i\frac{d^3\sigma}{d^3p_i}\delta(1-\cos\chi)\ , \qquad (3.46)$$

where $E_1E_2\,d^6\sigma/d^3p_1d^3p_2$ is the two-hadron inclusive cross section. The first sum on the right-hand side is over all distinct pairs of hadrons — $n(n-1)/2$ terms for an n-hadron final state. The second sum is a self-correlation (n terms) which guarantees the sum rule

$$\int_{-1}^{1} d\cos\chi\,\frac{1}{\sigma}\frac{d\Sigma}{d\cos\chi} = 1\ , \qquad (3.47)$$

since $\sum E_i = \sqrt{s}$. Eq. (3.46) represents the standard integrated version of the EEC, in the sense that the information concerning the orientation of the final state with respect to the beam direction has been integrated out. A related quantity is the *asymmetry* of the energy-energy correlation function (EECA), defined by

$$\frac{1}{\sigma}\frac{d\Sigma^A}{d\cos\chi} = \frac{1}{\sigma}\frac{d\Sigma}{d\cos\chi}\bigg|_{180°-\chi} - \frac{1}{\sigma}\frac{d\Sigma}{d\cos\chi}\bigg|_{\chi}\ , \qquad (3.48)$$

for $0 \leq \cos\chi \leq 1$, which, at least in principle, has smaller hadronization corrections (see Chapter 5). The EEC, therefore, measures the correlation of hadronic energy flow in an event. In a 'two-jet' event, for example, the function is strongly peaked at $\chi = 0°$ and $\chi = 180°$. In contrast, the more isotropic (spherical) the event, the flatter the distribution.

The energy-energy correlation function is straightforward to measure in experiments, relatively insensitive to hadronization and, most important from a theoretical point of view, infra-red safe. The cancellation of the singular contributions from soft and collinear real gluon emission and from virtual gluons can take place, since the net energy weighting and angular distribution is the same for both. At lowest order, $e^+e^- \to q\bar{q}$, the EEC is simply

$$\frac{1}{\sigma}\frac{d\Sigma}{d\cos\chi} = \frac{1}{2}\delta(1-\cos\chi) + \frac{1}{2}\delta(1+\cos\chi)\ . \qquad (3.49)$$

For $\chi \neq 0°, 180°$ the perturbation series starts at order α_S with the process $e^+e^- \to q\bar{q}g$, *i.e.*

$$\frac{1}{\sigma}\frac{d\Sigma}{d\cos\chi} = \frac{\alpha_S(\mu^2)}{2\pi}A_1(\chi) + \left(\frac{\alpha_S(\mu^2)}{2\pi}\right)^2 A_2\left(\chi, \frac{s}{\mu^2}\right) + \cdots\ . \qquad (3.50)$$

The first two terms in this series have been calculated [21]. In fact, A_1

Downloaded from https://www.cambridge.org/core. UNIVERSIDAD AUTONOMA METROPOLITANA, on 15 Nov 2026 at 06:22:37, subject to the Cambridge Core terms of use, available at https://www.cambridge.org/core/terms. https://doi.org/10.1017/CBO9780511628788.004

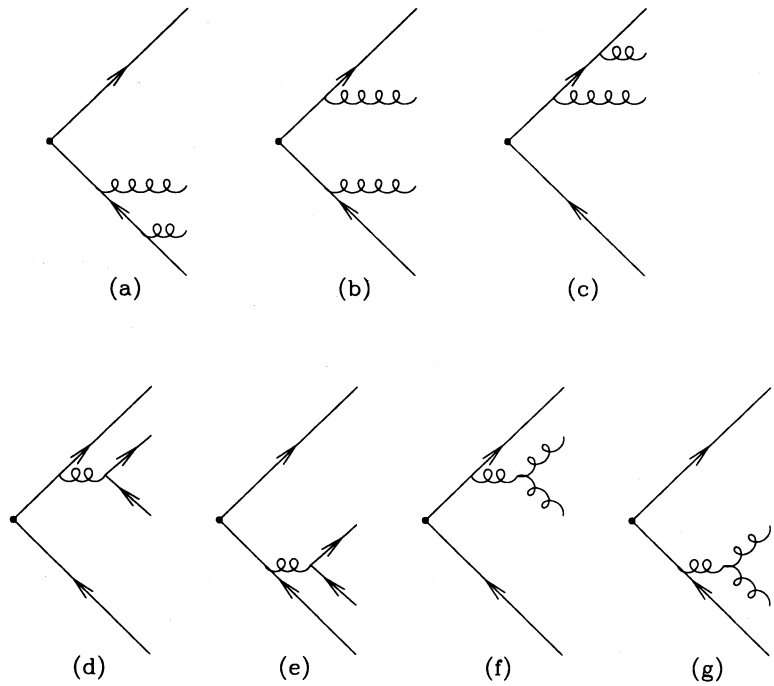


Fig. 3.10. Feynman diagrams for the $e^+e^- \to q\bar{q}gg$, $q\bar{q}q\bar{q}$ contributions to four-jet production in e^+e^- annihilation.

is obtained from the differential cross section given in Eq. (3.11) by including an appropriate δ-function expressing the angle χ in terms of the energy fractions x_i. The functions $A_i(\chi)$ are singular at $\chi = 0°, 180°$ but well away from these regions the series appears to converge satisfactorily. As for the other shape variables, resummation of large logarithmic contributions can extend the region of applicability into the singular regions.

3.5 The triple-gluon vertex

In the previous sections we have seen how cross sections can be defined for an arbitrary number of jets in the final state. We have seen in Fig. 3.7 that events containing as many as five jets have been identified at LEP. The four-jet rate is particularly interesting, since this is the lowest-order cross section in e^+e^- annihilation which is sensitive to the triple-gluon vertex, see Fig. 3.10.[8]

[8] The triple-gluon vertex also plays an important role in large p_T jet production at hadron colliders, through the $gg \to gg$ subprocess, see Chapter 7.

Downloaded from https://www.cambridge.org/core. UNIVERSIDAD AUTONOMA METROPOLITANA, on 15 Nov 2026 at 06:22:37, subject to the Cambridge Core terms of use, available at https://www.cambridge.org/core/terms. https://doi.org/10.1017/CBO9780511628788.004

Within the context of jet production in e^+e^- annihilation, we have seen how the three-jet cross section is consistent with a spin-one gluon. We could, however, imagine an alternative 'Abelian QCD' theory, in which SU(3) is replaced by $[U(1)]^3$, and the coupling is adjusted to be $\tilde{\alpha}_S = C_F\alpha_S$, so that the correct three-jet rate is obtained.[9] It is then the four-jet rate that allows this to be distinguished from QCD, since only a subset ((a) – (e)) of the Feynman diagrams shown in Fig. 3.10 contribute in the Abelian case.

The matrix elements corresponding to the diagrams in Fig. 3.10 were first calculated in ref. [24]. The general structure is

$$d\sigma^{(4)} = \left(\frac{\alpha_S}{2\pi}\right)^2 \left[C_F^2\mathcal{A} + C_F C_A \mathcal{B} + C_F T_R n_f \mathcal{C}\right] , \qquad (3.51)$$

where $\mathcal{A}$, $\mathcal{B}$ and $\mathcal{C}$ are functions of the parton-parton invariant masses squared, $s_{ij} = (p_i+p_j)^2$. The last term on the right-hand side of Eq. (3.51) corresponds to the $q\bar{q}q\bar{q}$ final state, and is common to both the Abelian and non-Abelian theories. The first two terms correspond to the $q\bar{q}gg$ final state: the second term receives contributions from the triple-gluon vertex diagrams and is absent in the Abelian theory.

With the overall couplings already fixed by the three-jet rate, the four-jet rates are therefore different in the two theories, and one could in principle discriminate between them on the basis of overall event rate alone. In particular, the rate is much smaller for the Abelian theory, where the $q\bar{q}q\bar{q}$ final state is relatively more important than in QCD. The problem with this is that the magnitude of the cross section is quite sensitive to the choice of scale in the strong coupling which appears in Eq. (3.51), and this freedom would allow the overall rates to be adjusted to fit the measured rate in each case. In principle, the fraction of four-quark events would also provide a discrimination. However, as we shall see in Chapter 6, it is very difficult to distinguish light-quark and gluon jets with the necessary efficiency. The only realistic possibility appears to be to tag at least three b quarks in the final state (using vertex detectors or semi-leptonic decays) to estimate the fraction of $q\bar{q}q\bar{q}$ events, but the efficiency is again very low.

A much more powerful and illuminating method makes use of the different *correlations* among the final-state particles induced by the various contributions to the cross section. These correlations have their origin in the different angular momentum properties of the final state, and will be discussed in more detail in Chapter 5. Several event shape variables have been proposed for using angular correlations to quantify the differences

[9] Such a theory is not, of course, asymptotically free, and is therefore already ruled out by data such as those shown in Fig. 3.6.

Downloaded from https://www.cambridge.org/core. UNIVERSIDAD AUTONOMA METROPOLITANA, on 15 Nov 2026 at 06:22:37, subject to the Cambridge Core terms of use, available at https://www.cambridge.org/core/terms. https://doi.org/10.1017/CBO9780511628788.004

between the Abelian and non-Abelian theories [25]. The basic idea is to measure the relative orientation of the planes containing the primary $q\bar{q}$ jets and the secondary gg or $q\bar{q}$ jets. Of course in practice one cannot distinguish primary and secondary jets on an event-by-event basis, but on average the secondary jets are less energetic, in the same way that the gluon in $q\bar{q}g$ production is the least energetic jet on average.

In practice, the most widely-used variables are the Nachtmann-Reiter angle θ_{NR}, defined by

$$\cos\theta_{NR} = \frac{(\boldsymbol{p}_1 - \boldsymbol{p}_3)\cdot(\boldsymbol{p}_2 - \boldsymbol{p}_4)}{|\boldsymbol{p}_1 - \boldsymbol{p}_3|\,|\boldsymbol{p}_2 - \boldsymbol{p}_4|}\,, \tag{3.52}$$

where the $\boldsymbol{p}_i$ are the jet three-momenta, ordered according to energy, and the Bengtsson-Zerwas angle χ_{BZ}, defined as the angle between the planes defined by the two lowest and two highest energy jets:

$$\cos\chi_{BZ} = \frac{(\boldsymbol{p}_1 \times \boldsymbol{p}_2)\cdot(\boldsymbol{p}_3 \times \boldsymbol{p}_4)}{|\boldsymbol{p}_1||\boldsymbol{p}_2||\boldsymbol{p}_3||\boldsymbol{p}_4|}\,. \tag{3.53}$$

Fig. 3.11 shows the χ_{BZ} distribution measured by the L3 collaboration at LEP [26]. The curves correspond to the Abelian and non-Abelian QCD theories, and the data exhibit a clear preference for the former.

3.6 Gluon emission from heavy quarks

The results for jet cross sections and shape variables presented so far have been derived assuming the quarks are massless. In this section we extend some of the previous $O(\alpha_S)$ results to heavy quarks. For pure vector s-channel exchange[10], *e.g.* $e^+e^- \to \gamma^* \to Q\overline{Q}g$, the cross section differential in the quark and antiquark energy fractions is, for a quark of mass m, (*cf.* Eq. (3.31))

$$\begin{aligned}\frac{1}{\sigma}\frac{d^2\sigma}{dx_1 dx_2} &= \frac{1}{\beta}C_F\frac{\alpha_S}{2\pi}\left[\frac{2(x_1+x_2-1-2\gamma)}{(1-x_1)(1-x_2)}\right.\\ &\quad -2\gamma\left\{\frac{1}{(1-x_1)^2}+\frac{1}{(1-x_2)^2}\right\}\\ &\quad \left.+\frac{1}{1+2\gamma}\,\frac{(1-x_1)^2+(1-x_2)^2}{(1-x_1)(1-x_2)}\right]\,,\end{aligned} \tag{3.54}$$

where

$$\gamma = \frac{m^2}{s} \le \frac{1}{4}, \qquad \beta = \sqrt{1-4\gamma}\,. \tag{3.55}$$

[10] Unlike for massless quarks, the $e^+e^- \to Q\overline{Q}g$ matrix element is different for s-channel vector and axial exchange, see ref. [27] for a full discussion.

Downloaded from https://www.cambridge.org/core. UNIVERSIDAD AUTONOMA METROPOLITANA, on 15 Nov 2026 at 06:22:37, subject to the Cambridge Core terms of use, available at https://www.cambridge.org/core/terms. https://doi.org/10.1017/CBO9780511628788.004

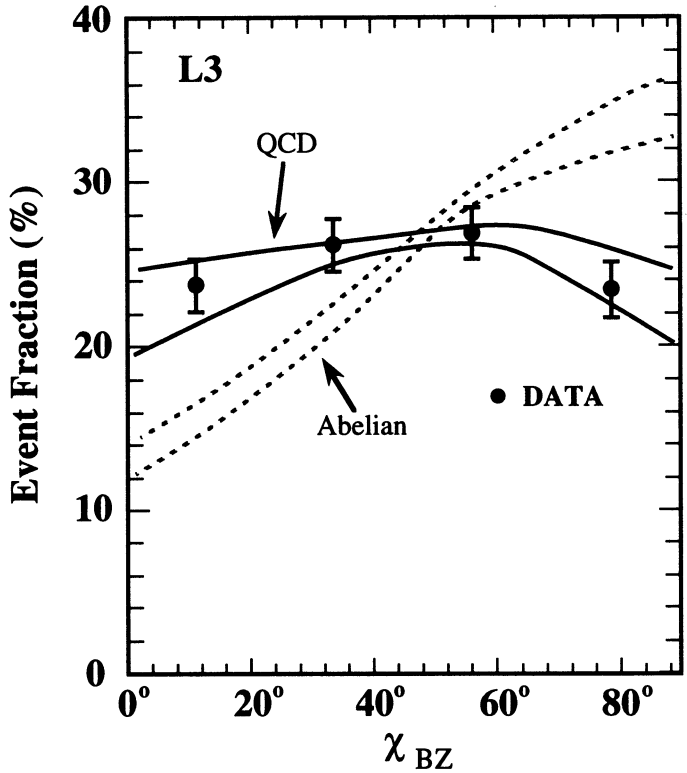


Fig. 3.11. Distribution in the Bengtsson-Zerwas angle at LEP. Figure from ref. [26].

Because the quarks have mass, the phase space available for gluon emission is reduced. As an illustration, the phase space boundary for the case $\gamma = 1/25$ ($m = \sqrt{s}/5$) is shown in Fig. 3.12. In the limit $\gamma \to 0$, the boundary expands to become the usual massless-quark triangle, $x_1 = 1$, $x_2 = 1$, $x_1 + x_2 = 1$, while for $\gamma \to 1/4$ — the heavy-quark threshold — the phase space shrinks to a point at $x_1 = x_2 = 1$. An important feature of the cross section in Eq. (3.54) is that the collinear divergences are regularized by the non-zero quark mass. From Fig. 3.12, we see that the singularities along the lines $x_1 = 1$ and $x_2 = 1$ are outside the phase space region. There is still, however, a single-logarithmic infra-red divergence when the gluon momentum approaches zero, *i.e.* at $x_1 = x_2 = 1$. Another interesting feature, not immediately apparent from Eq. (3.54), is that the cross section is suppressed near the phase space boundary, which corresponds to gluons approximately collinear with the heavy quarks. This is called the 'dead-cone' effect [28]. It is simply a reflection of the fact that angular momentum conservation suppresses the emission, via a helicity-

Downloaded from https://www.cambridge.org/core. UNIVERSIDAD AUTONOMA METROPOLITANA, on 15 Nov 2026 at 06:22:37, subject to the Cambridge Core terms of use, available at https://www.cambridge.org/core/terms. https://doi.org/10.1017/CBO9780511628788.004

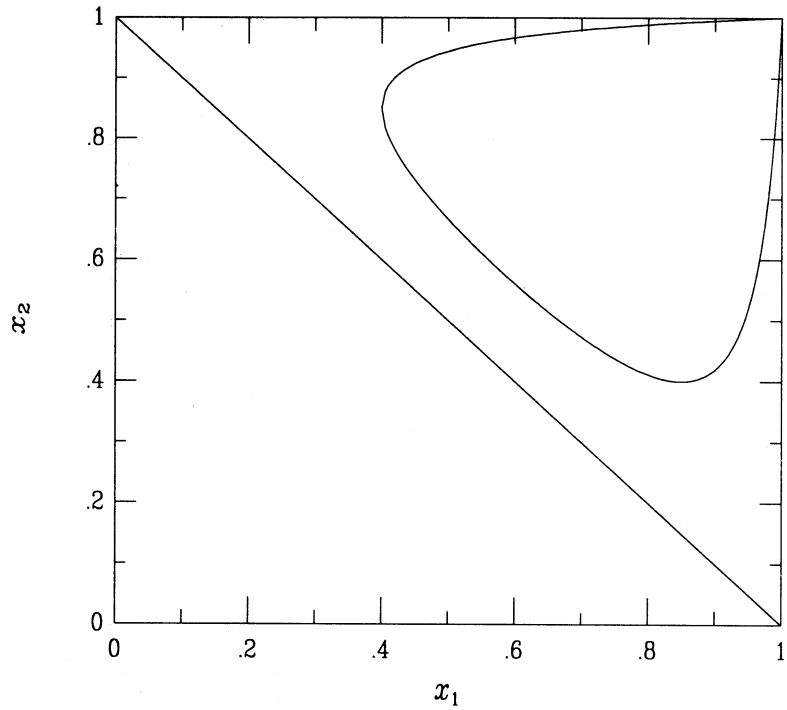


Fig. 3.12. The phase space boundary for $Q\overline{Q}g$ production in e^+e^- annihilation. The quark mass is $m = \sqrt{s}/5$.

conserving interaction, of a spin-one gluon in the same direction as a spin-$\frac{1}{2}$ quark. In fact for gluons which are soft ($z = 2 - x_1 - x_2 \ll 1$) and close in angle (θ) to the direction of motion of a heavy quark with $\gamma \ll 1$, the differential cross section in Eq. (3.54) can be approximated by

$$\frac{1}{\sigma}\frac{d^2\sigma}{dzd\theta^2} \approx C_F\frac{\alpha_S}{\pi}\frac{1}{z}\frac{\theta^2}{(\theta^2+4\gamma)^2}\,. \tag{3.56}$$

This shows that the gluon radiation is suppressed in an angular cone of size $\theta \sim 2\sqrt{\gamma} = 2m/\sqrt{s}$. In other words, the heavier the quark, the broader the dead cone.

The above results are derived under the assumption that the heavy quark is *stable*. In practice, heavy quarks like $c, b, t, \ldots$ decay weakly after a finite length of time, $Q \to qW^{(*)} \to qq\bar{q}, ql\nu$, and a complete analysis of gluon radiation associated with such quarks should also take into account the possibility of emitting gluons from the decay products. Further details can be found, for example, in ref. [29].

Downloaded from https://www.cambridge.org/core. UNIVERSIDAD AUTONOMA METROPOLITANA, on 15 Nov 2026 at 06:22:37, subject to the Cambridge Core terms of use, available at https://www.cambridge.org/core/terms. https://doi.org/10.1017/CBO9780511628788.004

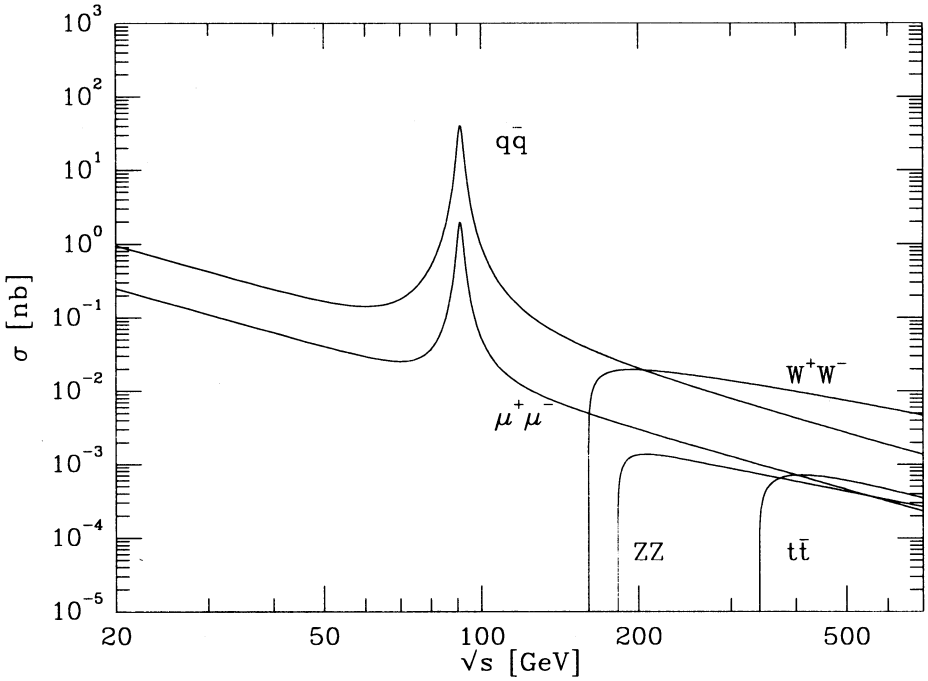


Fig. 3.13. Cross sections in e^+e^- annihilation.

3.7 Summary and outlook

Electron-positron annihilation into hadrons at high energy provides a particularly clean environment in which to test perturbative QCD. At the LEP and SLC colliders, for example, the energy is sufficiently high that for many quantities of interest, the corrections due to hadronization are small. Jet final states then give direct insight into the production and properties of the quarks and gluons. In such a way, the basic $q\bar{q}g$ and ggg interactions of the theory have been verified. The precision on measurements of $\alpha_S(M_Z^2)$ from the total hadronic cross section and from jet cross sections and shape variables is of order 5% (see Chapter 12).

The success of QCD studies at LEP and SLC is due in part to the fact that the peak hadronic cross section is so large, of order 40 nb, as shown in Fig. 3.13. Above the Z peak, the e^+e^- annihilation hadronic cross section falls away rapidly, ultimately regaining the $1/s$ fall-off of lower energies. This means that a future high-energy e^+e^- collider would find it difficult to match the precision of QCD studies at $\sqrt{s} = M_Z$. However, there would be other hadronic production processes with larger cross sections. Examples are the electroweak processes $e^+e^- \to W^+W^- \to$ jets and $\gamma\gamma \to$ jets. In fact, at the LEP2 collider ($\sqrt{s} = 160 - 200$ GeV) the QCD

Downloaded from https://www.cambridge.org/core. UNIVERSIDAD AUTONOMA METROPOLITANA, on 15 Nov 2026 at 06:22:37, subject to the Cambridge Core terms of use, available at https://www.cambridge.org/core/terms. https://doi.org/10.1017/CBO9780511628788.004

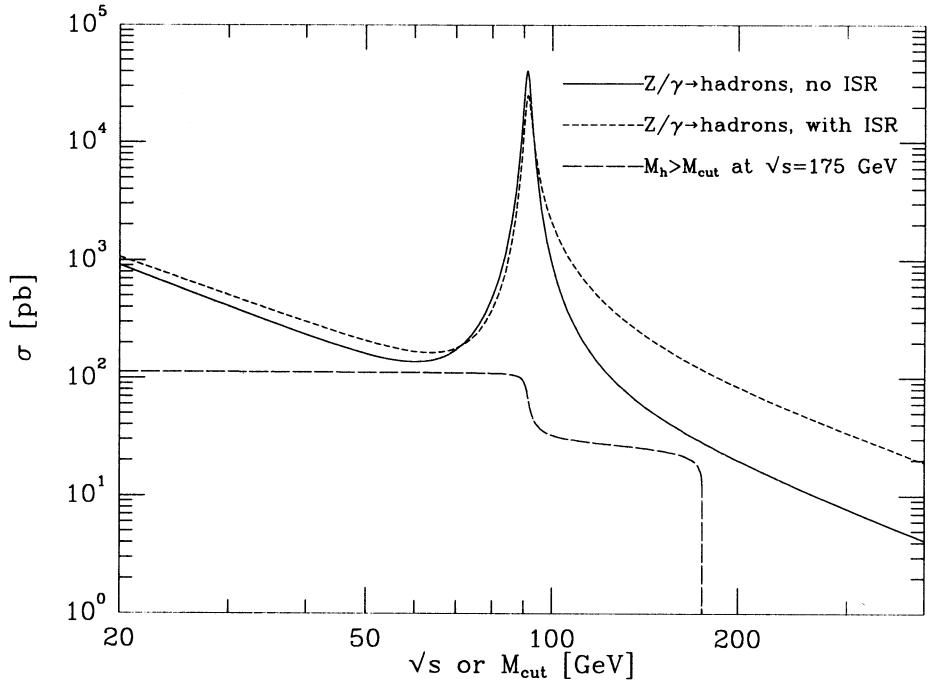


Fig. 3.14. Hadronic cross section with initial-state radiation. Adapted from ref. [31].

annihilation process $e^+e^- \to \sum q\bar{q} \to$ jets is a non-negligible *background* to the W mass determination from the $e^+e^- \to W^+W^- \to q\bar{q}q\bar{q}$ final state [30].

Another feature of the annihilation cross section which is relevant to LEP2 physics is the phenomenon known as 'radiative return to the Z pole'. By radiating one or more hard collinear photons, the incoming electron and/or positron can lose enough energy that the hadronic invariant mass M_h is close to the pole of the Z propagator, *i.e.* $\sqrt{s} > M_h \sim M_Z$. The enhancement of the cross section thus obtained more than compensates the additional powers of the electromagnetic coupling, so that $\sigma(e^+e^- \to \sum q\bar{q} + n\gamma) > \sigma(e^+e^- \to \sum q\bar{q})$. This may be seen by comparing the solid and short-dashed curves in Fig. 3.14.

Even though the radiated photons are usually too close to the beam direction to be detectable, events with hard initial-state radiation are relatively easy to eliminate by means of a lower cut on the hadronic invariant mass M_h. The long-dashed curve in Fig. 3.14 shows the cross section at fixed $\sqrt{s} = 175$ GeV, as a function of such a cut, $M_h > M_{cut}$. For $M_{cut} = 0$, the cross section coincides with the value on the dashed curve at $\sqrt{s} = 175$ GeV. As the cut is increased above the Z mass, the cross

Downloaded from https://www.cambridge.org/core. UNIVERSIDAD AUTONOMA METROPOLITANA, on 15 Nov 2026 at 06:22:37, subject to the Cambridge Core terms of use, available at https://www.cambridge.org/core/terms. https://doi.org/10.1017/CBO9780511628788.004

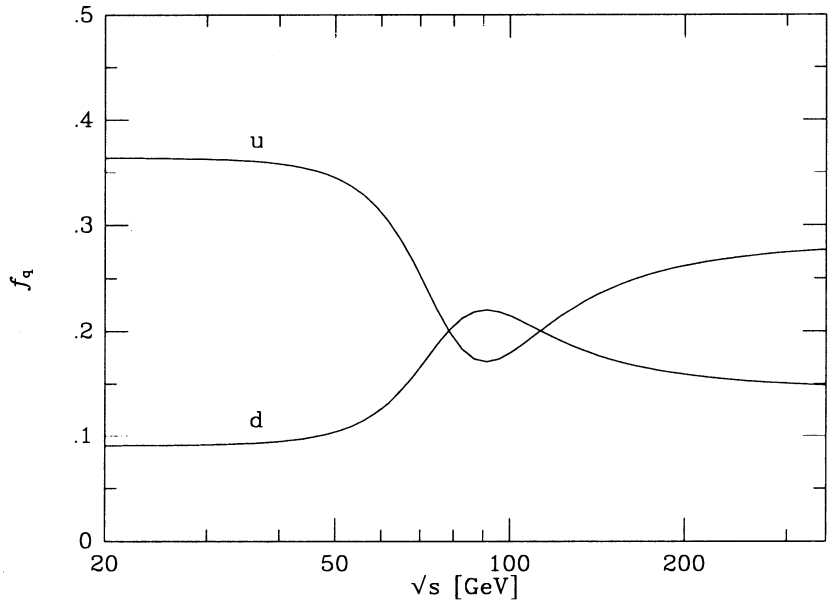


Fig. 3.15. u and d quark contributions as a fraction of the total $e^+e^- \to \sum q\bar{q}$ cross section, with $q = u, d, s, c, b$.

section drops suddenly, as a consequence of the 'radiative return' effect discussed above. It then remains fairly constant before falling sharply to zero at $M_{cut} = \sqrt{s}$. Thus, in the region $M_{cut} > M_Z$, the cross section remains close to the Born value, *i.e.* the value on the solid curve at $\sqrt{s} = 175$ GeV, provided one allows for at least a few GeV of initial-state radiation.

For two-photon induced hadronic events, $e^+e^- \to e^+e^- + \sum q\bar{q}$, the hadronic invariant mass is strongly peaked at small values, again making them relatively easy to distinguish from annihilation events by means of an invariant mass cut.

A final point concerns the relative proportions of u- and d-type quarks in the $e^+e^- \to \sum q\bar{q}$ annihilation cross section shown in Fig. 3.13. Because of the differences between the quarks' electric and weak (neutral current) charges, these proportions change as the energy of the collider increases. Fig. 3.15 shows the u and d quark contributions as a fraction of the total light-quark (*i.e.* (u, d, s, c, b)) cross section. At low energies ($\sqrt{s} \ll M_Z$) the fractions are essentially determined by the electric charges, and so $f_u \approx 4/11$, $f_d \approx 1/11$. As the energy increases, the Z-exchange contribution becomes more important (see Eq. (3.1)). The maximum value of f_d occurs at the Z peak, where $f_d > f_u$. Since above the $b\bar{b}$ threshold $f_b \approx f_d$, we see that the b quark fraction is also maximal at $\sqrt{s} \simeq M_Z$. At

Downloaded from https://www.cambridge.org/core. UNIVERSIDAD AUTONOMA METROPOLITANA, on 15 Nov 2026 at 06:22:37, subject to the Cambridge Core terms of use, available at https://www.cambridge.org/core/terms. https://doi.org/10.1017/CBO9780511628788.004

very high energies ($\sqrt{s} \gg M_Z$) the f_q fractions become constant again, with the values given by combinations of the electromagnetic and weak couplings.

References

1) D. Schaile, Proc. XXVII Int. Conf. on High Energy Physics, Glasgow, July 1994, eds. P.J. Bussey and I.G. Knowles, Institute of Physics Publishing, Bristol (1995), Vol. I, p. 27.

2) F. Bloch and A. Nordsieck, *Phys. Rev.* **52** (1937) 54.

3) T. Kinoshita, *J. Math. Phys.* **3** (1962) 650;
T.D. Lee and M. Nauenberg, *Phys. Rev.* **133B** (1964) 1549.

4) M.A. Samuel and L.R. Surguladze, *Phys. Rev. Lett.* **66** (1991) 560;
S.G. Gorishny, A.L. Kataev and S.A Larin, *Phys. Lett.* **B259** (1991) 144.

5) P.M. Stevenson, *Phys. Lett.* **B100** (1981) 61; *Phys. Rev.* **D23** (1981) 2916.

6) S.J. Brodsky, G.P. Lepage and P.B. MacKenzie, *Phys. Rev.* **D28** (1983) 228.

7) A. Djouadi, J.H. Kühn and P.M. Zerwas, *Zeit. Phys.* **C46** (1990) 411.

8) J. Schwinger, *Particles, Sources and Fields*, Addison-Wesley, New York (1973);
J. Jersak, E. Laermann and P.M. Zerwas, *Phys. Rev.* **D25** (1982) 1218;
L. Reinders, H. Rubenstein and S. Yazaki, *Phys. Rep.* **127** (1985) 1;
T.H. Chang, K.J.F. Gaemers and W.L. van Neerven, *Nucl. Phys.* **B202** (1982) 407.

9) S.G. Gorishny, A.L. Kataev and S.A Larin, *Nuovo Cimento* **92A** (1986) 117;
K.G. Chetyrkin, J.H. Kühn and A. Kwiatkowski, *Phys. Lett.* **B282** (1992) 221.

10) B.A. Kniehl and J.H. Kühn, *Phys. Lett.* **B224** (1989) 229; *Nucl. Phys.* **B329** (1990) 547.

11) G. Sterman and S. Weinberg, *Phys. Rev. Lett.* **39** (1977) 1436.

12) JADE collaboration, S. Bethke *et al.*, *Phys. Lett.* **B213** (1988) 235.

13) S. Bethke, Z. Kunszt, D.E. Soper and W.J. Stirling, *Nucl. Phys.* **B370** (1992) 310.

14) G. Kramer and B. Lampe, *Fortschr. Phys.* **37** (1989) 161.

15) OPAL collaboration, M.Z. Akrawy *et al.*, *Phys. Lett.* **B235** (1990) 389.

16) N. Brown and W.J. Stirling, *Phys. Lett.* **B252** (1990) 657.

17) S. Catani, Yu.L. Dokshitzer, M. Olsson, G. Turnock and B.R. Webber, *Phys. Lett.* **B269** (1991) 432.

18) S. Brandt, Ch. Peyrou, R. Sosnowski and A. Wroblewski, *Phys. Lett.* **12** (1964) 57;
E. Farhi, *Phys. Rev. Lett.* **39** (1977) 1587.

19) H. Georgi and M. Machacek, *Phys. Rev. Lett.* **39** (1977) 1237.

20) R.K. Ellis, D.A. Ross and A.E. Terrano, *Nucl. Phys.* **B178** (1981) 421.

21) Z. Kunszt *et al.*, *Z Physics at LEP1*, CERN Report 89-08 (1989), Vol. 1, p. 373.

22) DELPHI collaboration, P. Abreu *et al.*, *Zeit. Phys.* **C54** (1992) 55.

23) C.L. Basham, L.S. Brown, S.D. Ellis and S.T. Love, *Phys. Rev. Lett.* **41** (1978) 1585.

24) A. Ali, J.G. Körner, G. Kramer, Z. Kunszt, E. Pietarinen, G. Schierholz and J. Willrodt, *Phys. Lett.* **B82** (1979) 285; *Nucl. Phys.* **B167** (1980) 454.

25) J.G. Körner, G. Schierholz and J. Willrodt, *Nucl. Phys.* **B185** (1981) 365;
O. Nachtmann and A. Reiter, *Zeit. Phys.* **C14** (1982) 47; *ibid.* **C16** (1982) 45;
M. Bengtsson and P.M. Zerwas, *Phys. Lett.* **B208** (1988) 306;
M. Bengtsson, *Zeit. Phys.* **C42** (1989) 75.

26) L3 collaboration, B. Adeva *et al.*, *Phys. Lett.* **B248** (1990) 227.

27) Yu.L. Dokshitzer, V.A Khoze and W.J. Stirling, *Nucl. Phys.* **B428** (1994) 3.

Downloaded from https://www.cambridge.org/core. UNIVERSIDAD AUTONOMA METROPOLITANA, on 15 Nov 2026 at 06:22:37, subject to the Cambridge Core terms of use, available at https://www.cambridge.org/core/terms. https://doi.org/10.1017/CBO9780511628788.004

28) Yu.L. Dokshitzer, V.A. Khoze, and S.I. Troyan, *Proc. 6th Int. Conf. on Physics in Collision*, ed. M. Derrick, World Scientific (1987), p. 417.

29) G. Jikia, *Phys. Lett.* **B257** (1991) 196;
V.A. Khoze, L.H. Orr and W.J. Stirling, *Nucl. Phys.* **B378** (1992) 413.

30) Report of the *W* Mass Working Group, in *Physics at LEP2*, eds. G. Altarelli, T. Sjöstrand and F. Zwirner, CERN Report 96-01 (1996).

31) P. Nason, in *Physics at LEP2*, eds. G. Altarelli, T. Sjöstrand and F. Zwirner, CERN Report 96-01 (1996).

Downloaded from https://www.cambridge.org/core. UNIVERSIDAD AUTONOMA METROPOLITANA, on 15 Nov 2026 at 06:22:37, subject to the Cambridge Core terms of use, available at https://www.cambridge.org/core/terms. https://doi.org/10.1017/CBO9780511628788.004